Dynamics of matter-wave condensates with time-dependent two- and three-body interactions trapped by a linear potential in the presence of atom gain or loss

D. Belobo Belobo,[1,*] G. H. Ben-Bolie,[1,2,†] and T. C. Kofane[2,3,4,‡]

[1]*Laboratory of Atom and Radiation, Department of Physics, Faculty of Science, University of Yaounde I, P.O. Box 812, Yaounde, Cameroon*

[2]*Centre d'Excellence en Technologies de l'Information et de la Communication (CETIC), University of Yaounde I, Yaounde, Cameroon*

[3]*Laboratory of Mechanics, Department of Physics, Faculty of Science, University of Yaounde I, P.O. Box 812, Yaounde, Cameroon*

[4]*The Abdus Salam International Center for Theoretical Physics, Strada Costiera 11, 34014 Trieste, Italy*

(Received 31 August 2013; revised manuscript received 15 February 2014; published 21 April 2014)

Bose-Einstein condensates with time varying two- and three-body interatomic interactions, confined in a linear potential and exchanging atoms with the thermal cloud are investigated. Using the extended tanh-function method with an auxiliary equation, i.e., the Lenard equation, many exact solutions describing the dynamics of matter-wave condensates are derived. An important issue is the time management of the cubic and the quintic nonlinearities by tuning the rate of exchange of atoms between the condensate and the thermal background. In addition, adjusting the strength of the linear potential, the rate of exchange of atoms, and many other free parameters allow one to control many features of the condensate such as its height, width, position, velocity, acceleration, and its direction, respectively. Full numerical solutions corroborate the analytical predictions.

DOI: 10.1103/PhysRevE.89.042913 PACS number(s): 05.45.Yv, 03.75.Lm, 03.75.Kk, 34.20.Cf

I. INTRODUCTION

The experimental observation of Bose-Einstein condensates (BECs) of trapped atomic vapors [1–3] has allowed investigations of some fundamental concepts of atomic physics and condensed matter physics [4]. Among these concepts, the question of how to control the dynamics of collective assemblies of atoms that are in the same quantum state is of great importance. It is well known that at very low temperatures, the dynamical behavior of a BEC is well described by the Gross-Pitaevskii equation (GPE) [4] which is a nonlinear Schrödinger equation with an external potential. The GPE exhibits many types of nonlinear excitations such as dark solitons [4], bright solitons [4], compactons [5], and so on. All the nonlinear phenomena observed in matter-wave condensates can be better explained with exact analytical solutions of the GPE. So, finding exact solutions of the GPE is a task of relative importance. For example, exact solutions may (i) help to choose appropriate experimental parameters, (ii) provide a way for probing the validity of the GPE at higher densities, (iii) help to analyze the stability of condensates, (iv) check the numerical analysis of the GPE, and (v) help to explain the formation and the propagation of different kinds of patterns in BECs as well as their long-time evolution. In the past few decades, many methods have been used to exactly solve the GPE such as the inverse scattering transform method [6], the mapping deformation method [7], and the extended tanh-function method [8], just to name a few. The extended tanh-function method is an approximate method used to exactly solve nonlinear partial differential equations. This method is a good technique for constructing exact or approximate traveling wave solutions of nonlinear wave equations arising in physics. The basic idea of the method is to choose a trial wave function with some free parameters that have important physical significance. The trial wave function is associated with an auxiliary equation (which has known exact solutions) that depends on a traveling variable. For example, Riccati equation $\phi' = A + \phi^3$, auxiliary ordinary equation $\phi'^2 = B\phi^2 + C\phi^2 + D\phi^4$, first kind elliptic equation $\phi'^2 = A + B\phi^2 + D\phi^4$, the generalized Riccati equation $\phi' = r + p\phi + q\phi^2$, and so on [9]. Using the chain rule for the derivations, the original nonlinear partial differential wave equation is converted into a set of ordinary differential equations which can be solved with symbolic computer algebra. The method furnishes not only qualitative but also quantitative results [9,10]. The validity of exact solutions found with the extended tanh-function method should be confirmed by some numerical integrations of the original equation.

In the GPE, nonlinearities arise from two-body interactions characterized by the scattering length, and by three-body collisions among atoms of the cloud. Some recent experiments have proved that the strength and the sign of the scattering length can be varied by using the so-called Feshbach resonance technique [11,12]. This has opened up many opportunities for the manipulation of matter-wave condensates and nonlinear excitations in BECs [13]. In most cases, the GPE describes condensates dominated by only the two-body interactions. In Ref. [14], the number of three-body interactions has been increased by using a magnetic field. The three-body interactions may become important and are used to describe the dynamics of condensates in the Tonks-Girardeau regime when the interatomic interactions are strong [15,16]. It has been shown in Refs. [17,18], that the two-body interactions and the three-body collisions can be managed separately. Recently, Mohamadou *et al.* [9] and Wamba *et al.* [10] proposed exact soliton solutions of the GPE with two-and three-body interactions by using a further extension of the tanh-function method that takes into account the three-body interactions. In this work, using the extended tanh-function method, we propose general exact solutions of the cubic-quintic GPE with time varying two-and three-body interatomic interactions.

*Corresponding author: belobodidier@gmail.com
†gbenbolie@yahoo.fr
‡tckofane@yahoo.com

As we will show below, the time-dependent interatomic interactions take into account the exchange of atoms between the BEC and the thermal cloud. The condensate is trapped in a linear potential that may also mimic the effects of the gravitational field. In BEC experiments, the linear potential can be produced by an appropriate magnetic gradient field, or an exposure of the BEC to an adequate optical laser field. A complex potential is also added phenomenologically in order to account for the exchange of atoms with the vapor background. Solutions presented here are very general ones with many free parameters that are used to control the dynamics of the BEC.

The paper is organized as follows. In Sec. II, we present the model and derived exact families of solutions. Then, we discuss the characteristics and evolution of matter-wave patterns. The stability of our exact solutions against small perturbations is studied in Sec. III. Then, with intensive numerical simulations, we investigate the dynamical properties of our exact analytical solutions in Sec. IV. Finally, Sec. V concludes the paper.

II. MODEL AND EXACT SOLUTIONS

At the mean-field level, the dynamics of one-dimensional BECs with both two- and three-body nonlinearities can be described by the following dimensionless GPE [19–23]:

$$\imath\Psi_t(x,t)+\Psi_{xx}-g(t)|\Psi(x,t)|^2\Psi(x,t) -\chi(t)|\Psi(x,t)|^4\Psi(x,t)-(\lambda x+\imath\gamma)\Psi(x,t)=0, \quad (1)$$

where the spatial coordinate x and the time coordinate t are measured in units of $\varsigma = 1\ \mu$m (the characteristic length unit in this type of experiment) and $m\varsigma^2/\hbar$, respectively, with m being the mass per particle. The time-dependent scattering length function $g(t)$ represents the strength of the two-body interactions. The function $\chi(t)$ takes into account the intensity of the three-body interactions and is in general a complex quantity; its imaginary part representing inelastic collisions can be neglected as shown by some recent works [24–30]. The cubic (quintic) nonlinearity is attractive if $g(t) < 0$ ($\chi(t) < 0$), while it is repulsive when $g(t) > 0$ ($\chi(t) > 0$). The parameter λ corresponds to the strength of a linear potential (or the gravitational field). The quantity γ is a parameter related to the exchange of atoms between the condensate and the uncondensed fraction of the thermal cloud. Positive values of γ correspond to the physical situation where atoms are fed into the condensate from the thermal background or injected into the condensate from a reservoir by a pumping mechanism [31,32]. Negative values of γ are related to atoms escaping out of the condensate due to dipolar relaxation [32]. In this case, the magnetic dipole-dipole interaction between the magnetic moments of two colliding atoms makes one or both atoms emerge from the collision in a different spin state, a process that induces an increase of the temperature of the BEC resulting in the expulsion of many atoms out of the trap [32]. Generally speaking, the dissipative mechanism corresponding to γ negative is spatially dependent [33]. The specific case where the rate of exchange of atoms is constant means that the size of the uncondensed fraction of atoms is larger than that of the condensate. The rate of exchange of atoms is characterized by a temporal scale ζ which is the time interval between subsequent events of adding or removing individual atoms from the atomic ensemble. The mean-field approximation remains valid if ζ is negligible, i.e., $\zeta\omega_\perp \ll 1$, which is verified for typical configurations where $\omega_\perp = 2\pi \times 360$ Hz and $\zeta \sim 4\ \mu$s [34]. This means that $|\gamma|$ is small. We prove below that the strengths of both the cubic nonlinearity $g(t)$ and the quintic nonlinearity $\chi(t)$ capture the exchange of atoms between the BEC and the background. Although the zero-temperature mean-field picture has been proven to provide good experimental results, one has to notice that experiments are carried out at finite temperatures where the thermal cloud is present. There are some regimes where the impact of the thermal cloud on the dynamical behavior of the condensate becomes important; for example, the problem of condensate growth, the heating of the gas under strong external perturbations, or the phase fluctuations exhibited by the condensate in low-dimensional systems. In such situations, Eq. (1) is coupled to another one describing the thermal cloud. Many models has been developed in order to account for effects of the thermal cloud. A tutorial review of these models with their physical relevance can be found in [35].

In order to obtain exact solutions of Eq. (1), we assume that the solution can be written as

$$\Psi(x,t) = h(t)\phi(\xi)\exp\left[\imath\theta(x,t)\right], \quad (2)$$

where $h(t)$ is a real function of time t, and $\xi = k(t)x + \eta(t)$ is the traveling wave variable, with $k(t)$ controlling the width of the condensate. The overall phase is $\theta = \Gamma(t)x + \Omega(t)$. The function $\Gamma(t)$ is the spatial frequency shift and $\Omega(t)$ is the homogeneous phase shift. Functions $h(t)$, $k(t)$, $\eta(t)$, $\Gamma(t)$, $\Omega(t)$, $\phi(\xi)$, $g(t)$, and $\chi(t)$ are unknown functions to be determined later. Following Refs. [10,36], we also assume that the unknown function $\phi(\xi)$ is the solution of the following auxiliary equation that considers the quintic nonlinearity

$$\left(\frac{d\phi}{d\xi}\right)^2 = b_0 + b_2\phi^2 + b_4\phi^4 + b_6\phi^6. \quad (3)$$

When one uses an auxiliary equation that is a polynomial in order to solve nonlinear partial differential equations where the the degree of the highest nonlinearity is "p" similar to Eq. (1), the order of the auxiliary equation should be "$p+1$" in order to have nontrivial solutions. The coefficient of the highest nonlinear term of the underlying equation to solve [here Eq. (1)] is proportional to the coefficient of the highest monomial of the auxiliary equation, as one can see in Eq. (9) below. Inserting Eq. (2) into Eq. (1) and collecting coefficients of powers $x^n\phi^l$ ($n = 0,1$, $l = 0,1,2,3,4,5$) and $\sqrt{b_0 + b_2\phi^2 + b_4\phi^4 + b_6\phi^6}$, then setting each of the coefficients to zero yields the following set of overdetermined partial differential equations where the "dot" denotes the derivative with respect to time t:

$$\begin{aligned} \dot{h} - \gamma h &= 0, \\ h(\dot{\eta} + 2\Gamma k) &= 0, \\ h\dot{k} &= 0, \\ h(-\dot{\Omega} + k^2 b_2 - \Gamma(t)^2) &= 0, \end{aligned}$$

$$h(\dot{\Gamma} + \lambda) = 0,$$
$$h[2b_4k^2 - g(t)h^2] = 0,$$
$$h[3k^2b_6 - \chi(t)h^4] = 0. \quad (4)$$

Solving the set of equations (4) with MAPLE we obtain

$$h(t) = C_5 \exp(\gamma t), \quad (5)$$

$$\Gamma(t) = -\lambda t + C_4, \quad (6)$$

$$k(t) = C_3, \quad (7)$$

$$g(t) = \frac{2b_4k^2(t)}{h^2(t)}, \quad (8)$$

$$\chi(t) = \frac{3b_6k^2(t)}{h^4(t)}, \quad (9)$$

$$\eta(t) = -2C_3\left(\frac{-\lambda t^2}{2} + C_4 t\right) + C_2, \quad (10)$$

$$\Omega(t) = -\left(\frac{\lambda^2 t^3}{3} - C_4\lambda t^2\right) + \left(b_2C_3^2 - C_4^2\right)t + \frac{C_4^3}{3\lambda} + C_1. \quad (11)$$

Coefficients C_1, C_2, C_3, C_4, C_5 are free real constant parameters related to the initial condition of the wave, such as initial coordinate, velocity, shape, amplitude, and overall phase. More importantly, in this work, we will try to find explicit ways to control the dynamical evolution of waves. From relations (6) and (11), one infers that the overall phase θ that is essential for reliable solutions does not depend on the rate of exchange of atoms between the condensed and uncondensed fractions. Adding or removing atoms from the condensate does not affect the direction of propagation of solutions. On the contrary, the linear potential deeply affects the overall phase θ of the condensate. Once the strength of the linear potential is fixed, as time evolves, the deviation of the linear frequency shift from its initial value C_4 is proportional to λ [see Eq. (6)], meanwhile the variation of the homogenous phase clearly depends on λ [see Eq. (8)]. The parameter b_2 is related to the solution pattern (see the Appendix). If the solution pattern is chosen, we can evaluate analytically the overall phase at each time from the initial condition. Hence, Eqs. (6) and (8) tell us how to adjust the strength of the linear potential in order to obtain a desired phase of the solution during evolution. Equations (5), (8), and (9) imply that the two- and three-body interactions are time dependent and also depend on the rate of exchange of atoms process with the thermal cloud. During evolution, the interplay between the BEC and the uncondensed fraction modulates the intensity of both two- and three-body interatomic interactions in the condensate. Furthermore, from Eqs. (8) and (9), one realizes that our solutions apply only for specific time-dependent behavior of the two- and three-body nonlinearities given by Eqs. (8) and (9), respectively. The expression of the two-body nonlinearity strength suggests the management of the two-body collisions, which can be controlled externally in BEC experiments by using the Feshbach resonance technique [11,12]. Equation (8) is similar to the expression of the scattering length obtained in Ref. [37] [$g(t) = a_0 \exp(\lambda t)$, a_0 being a constant] that was derived from the BEC experiments of Bradley *et al.* [2,38] where bright solitons were produced. Moreover, the two-body nonlinearity has also been tuned from repulsive to attractive in recent condensate experiments [39,40]. It has been shown in Ref. [41] that bright and dark solitons may be produced in the latter experiments ([39,40]) provided that the two-body nonlinearity takes a mathematical form close to that of Eq. (8). Apart from the fact that the two-body collisions can be time dependent, the three-body interactions can also be tuned via the Feshbach resonance technique [14]. Anticipating the experiments, some authors have proposed a periodic modulation of the coefficient of the three-body nonlinearity. In Ref. [42], such a time periodic variation of the three-body interatomic collisions has been used to analyze the stability of condensates with both two- and three-body interactions. Recently, a space modulation of the three-body nonlinearities has been used to stabilize one-dimensional condensates against critical collapse in quintic nonlinear lattices [43]. In this work, the three-body interatomic interactions strength $\chi(t)$ presents a similar behavior as the two-body nonlinearity $g(t)$. When the condensate is in the feeding regime ($\gamma > 0$), setting the parameters b_4 and b_6 to convenient values allows one to increase the intensity of the three-body interactions, allowing one to mimic the Tonks-Girardeau regime, where the three-body interactions dominate over the two-body collisions [14,15]. By inducing a time modulation, the exchange of atoms process considerably alters the cubic and quintic nonlinearities. After selecting the values of b_4 and b_6 which are related to the solution pattern needed (see the Appendix), the experimenter knows how to manage both the two- and three-body interatomic interactions in the BEC. Therefore, we can know how to adjust the related operations to control the evolution of the solutions' overall phase as well as the two- and three-body interatomic nonlinearities. It is clear that the linear potential does not play any role in the interaction among particles in the condensate. We deduce from Eq. (7) that the width of a solution, $1/C_3$, remains constant during evolution leading to the compression of the condensate when atoms are added in the system, while an amplitude dissipation will be observed if atoms are ejected out of the system. On the other hand, the choice of the free parameters b_4 and b_6 (b_4 and b_6 may take a wide range of values) and that of γ can be done in order to bring the BEC in the range of parameters used in current BEC experiments. In addition, one has to keep in mind the fact that in most recent works, the condensate was confined in an external parabolic potential [2,38–43], where the time management of the cubic nonlinearity was related to the strength of the parabolic potential, which was set to be a factor of the rate of the exchange of atoms with the thermal background. In this work, the quintic nonlinearity which is an exponential function of time, may be controlled by adjusting the feeding or loss of atoms process parameter γ, in a BEC dominated by a linear potential. We believe that such an exponential time-dependent quintic nonlinearity may motivate its realization in BEC experiments in the future. Moreover, in previous works, the expressions of the cubic and quintic nonlinearities are fixed, and then exact solutions

of the GPE are found [5,22,23,37,42–45]. In this work, we adopt a rather different approach by constructing both exact solutions of the GPE, and their corresponding expressions of the cubic and quintic nonlinearities. For the case at hand, the physical relevance of the expressions of the cubic and quintic nonlinearities as discussed above may be implemented in condensate experiments. Our approach may be used to find exact solutions of the GPE with different trap geometries, and may also be generalized to higher dimensions. An approach similar to the one presented in this work, but employing the Hirota bilinear method, has been used to derive exact solutions of a class of complex Ginzburg-Landau equations with time variable coefficients [46]. As in Eq. (1), the cubic nonlinearity is only prescribed to be time dependent in Ref. [46]; then its explicit expression as well as exact solutions are derived at the end of the calculations. In addition, when $b_4 < 0$ ($b_6 < 0$) the two-body (three-body) interactions are attractive, but for $b_4 > 0$ ($b_6 > 0$), the two-body (three-body) interactions are repulsive. Considering the solutions of the Lenard equation [Eq. (3)] given in the Appendix, we obtain a series of 22 families of exact solutions of Eq. (1) as

$$\Psi_{jp}(x,t) = h(t)\phi_{jp}(\xi)\exp\{\iota\,[\Gamma(t)x + \Omega(t)]\}\,. \tag{12}$$

The integer j corresponds to a family of solutions of Eq. (3) and varies from 1 to 11, while the integer p accounts for a particular solution of a specific family and may take the values 1, 2, and 3 [see solutions of Eq. (3) above]. A classification of different exact solutions and their characteristics (attractive or repulsive two- or three-body interactions) of Eq. (3) constructed in this work are regrouped in Table I.

The function $h(t)$ captures the strength of the interactions among atoms of the condensate. In the case where the BEC gains atoms ($\gamma > 0$), $h(t)$ increases meaning that the density of the matter wave increases too. On the contrary, $h(t)$ decreases and the density of the condensate reduces when the BEC loses atoms ($\gamma < 0$). Similar behaviors, which are in agreement with the physical reality, have been reported in Refs. [37,47]. Hence, a proper choice of the parameter γ may help to obtain an assumed peak without explosion of the condensate. The interplay between the condensate and the thermal background can be externally controlled and also modifies the amplitude of the solutions. Furthermore, large values of $|C_5|$ induce an increase of the condensate's density. Thus, it is possible to master the density of the condensate by adjusting the free parameter C_5. The selection of C_5 and that of the experimental parameter γ provide two powerful tools to control the amplitude of the solutions. Families of exact solutions also present many other interesting characteristics.

Setting the traveling variable to zero, $\xi = 0$, enables one to derive the position, velocity, and the acceleration of the center of mass of the matter wave as

$$\begin{aligned} x &= -\lambda t^2 + 2C_4 t - C_2/C_3, \\ \dot{x} &= -2\lambda t + 2C_4, \\ \ddot{x} &= -2\lambda. \end{aligned} \tag{13}$$

Equation (13) teaches us important things about the evolution at mean from the initial condition of three main properties of the solutions. First, the motion is characterized by the width and the strength of the linear potential λ. The center of mass of the condensate describes a parabola in the plane (t,x) with a constant acceleration, $2|\lambda|$, which is twice the strength of the linear potential λ. The relevant physical parameters that affect the motion and velocity of the solution are the strength of the linear potential λ and the solution's width. Secondly, we can compute the velocity and the acceleration of the center of mass of the solutions analytically. Thirdly, according to Newton's second law, the last equation of (13) formally corresponds to the classical equation of motion of a particle moving in the effective potential $2\lambda x$ with total energy $(1/2)\dot{x}^2 + 2\lambda x$, its only equilibrium point being zero. Hence, the presence of the linear potential induces an acceleration of the condensate. This feature may be used in some BEC applications such as the realization of the atomic laser where the velocity of atoms can be tuned by selecting the strength of the linear potential. Another potential application is the transport of the condensate in experiments driven by the parameter λ. The linear potential profoundly affects the motion of the center of mass of the condensate. At mean, our solutions are set into motion by the external potential which also induces a gradient on the condensate and finally modifies the trajectory of the condensate. In the absence of the linear potential ($\lambda = 0$), the center of mass of the BEC describes a straight line in the plane (t,x) and moves at a constant velocity that depends on the value of the free parameter C_4. The initial velocity of the wave is equal to $2 \mid C_4 \mid$. In addition, Eq. (12) presents many kinds of solutions with rather different shapes. Let us examine some of them in detail.

TABLE I. Classification of different solutions.

Type	j	p	Two-body interactions	Three-body interactions	δ
Trigonometric functions	2	1, 2	Repulsive	Attractive	Positive
	7		Attractive or repulsive	Attractive or repulsive	Positive
	9	1, 2	Attractive or repulsive	Repulsive	
Hyperbolic functions	1	1, 2	Attractive	Attractive	Positive
	3	1, 2	Attractive	Repulsive	
	4	1, 2	Attractive or repulsive	Attractive or repulsive	
	5		Attractive or repulsive	Attractive or repulsive	Positive
	8	1, 2	Attractive or repulsive	Repulsive	
	11		Attractive	Repulsive	
Exponential functions	4	3	Attractive or repulsive	Attractive or repulsive	
	10		Absence	Attractive or repulsive	

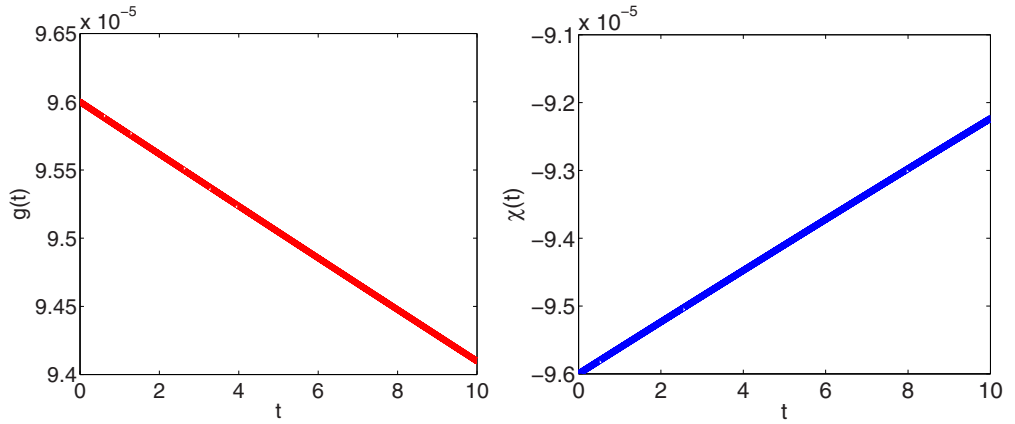

FIG. 1. (Color online) Temporal evolutions of repulsive cubic nonlinearity [panel (a)] and the attractive quintic nonlinearity [panel (b)]. Parameters are fixed as $\gamma = -0.001$, $C_3 = 0.1$, $b_4 = 3$, and $b_6 = -2$.

A. Periodic solutions

It is possible to generate a periodic solution by setting $j = 2$ and $p = 1$ in Eq. (12) with the following coefficients: $b_2 = -1$, $b_4 = 3$, $b_6 = -2$, $\gamma = -0.001$, and $\lambda = 0.001$. The other parameters are $C_5 = 1$, $C_4 = 0$, $C_2 = 0$, and $C_1 = 0$. The condensate is repulsive since $b4 > 0$, and is in the regime of loss of atoms. We display in Fig. 1 the temporal variations of the cubic nonlinearity [Fig. 1(a)], and the quintic nonlinearity [Fig. 1(b)]. One observes that the intensity of the cubic nonlinearity decreases, while the intensity of the quintic nonlinearity increases slightly faster. Figure 1 provides a way to understand how to modulate the cubic and the quintic nonlinearities in order to obtain localized solutions. Hence, using the Feshbach resonance management, the experimenter tunes the strengths of the cubic and the quintic nonlinearities by acting on the rate of exchange of atoms γ. In Fig. 2(a), the spatiotemporal evolution of the condensate's density shows a spatial periodic localized wave packet. The number of solitons, n, with the width, W_s, available on the cigar axis of length, L, can be determined with the formula

$$n = \left(\frac{L}{W_s}\right)\alpha, \tag{14}$$

where α is a real parameter used to scale the value of n. In Fig. 2(b) where $C_3 = 0.008$, the number of solitons is twice that in Fig. 2(a), in full agreement with the prediction of Eq. (14). It is possible to tune the periodicity of the solution to the desired value. We recall that such periodic solutions, moving at a constant acceleration presented in Fig. 2, are likely to be observed for condensates loaded in optical lattices. Nowadays, BECs can be produced in optical lattices which allow the management of many BEC properties such as the cubic and the quintic nonlinearities [48]. In BEC applications, the solutions presented in Fig. 2 can be used to insert atoms onto optical devices, such as atom chips, waveguides, and mirrors [48,49].

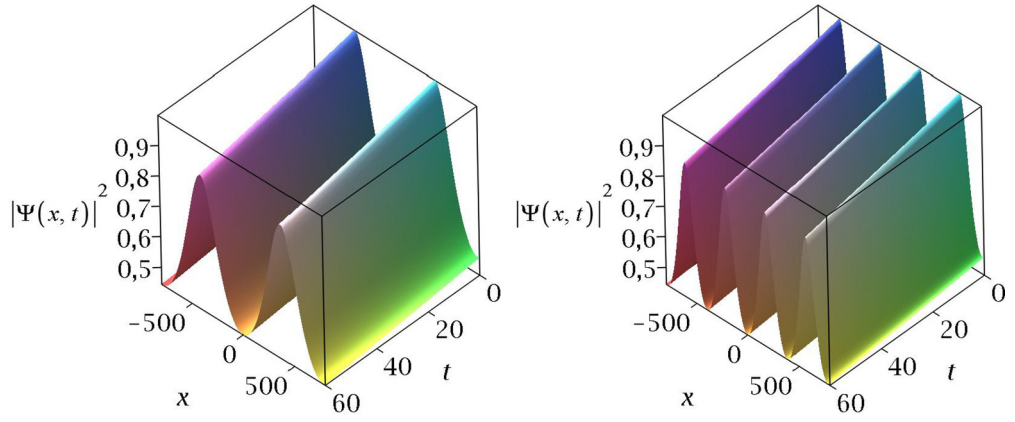

FIG. 2. (Color online) Periodic solution of Eq. (12) for $j = 2$, $p = 1$, $\lambda = 0.001$, $C_3 = 0.004$, $b_2 = -1$, $C_5 = 1$, and $C_1 = C_2 = C_4 = 0$. (a) Spatiotemporal dynamics of the wave function in the regime of atoms loss, $\gamma = -0.001$. (b) Control of the number of solitons, $W = 0.008$. The other parameters correspond to those in Fig. 1.

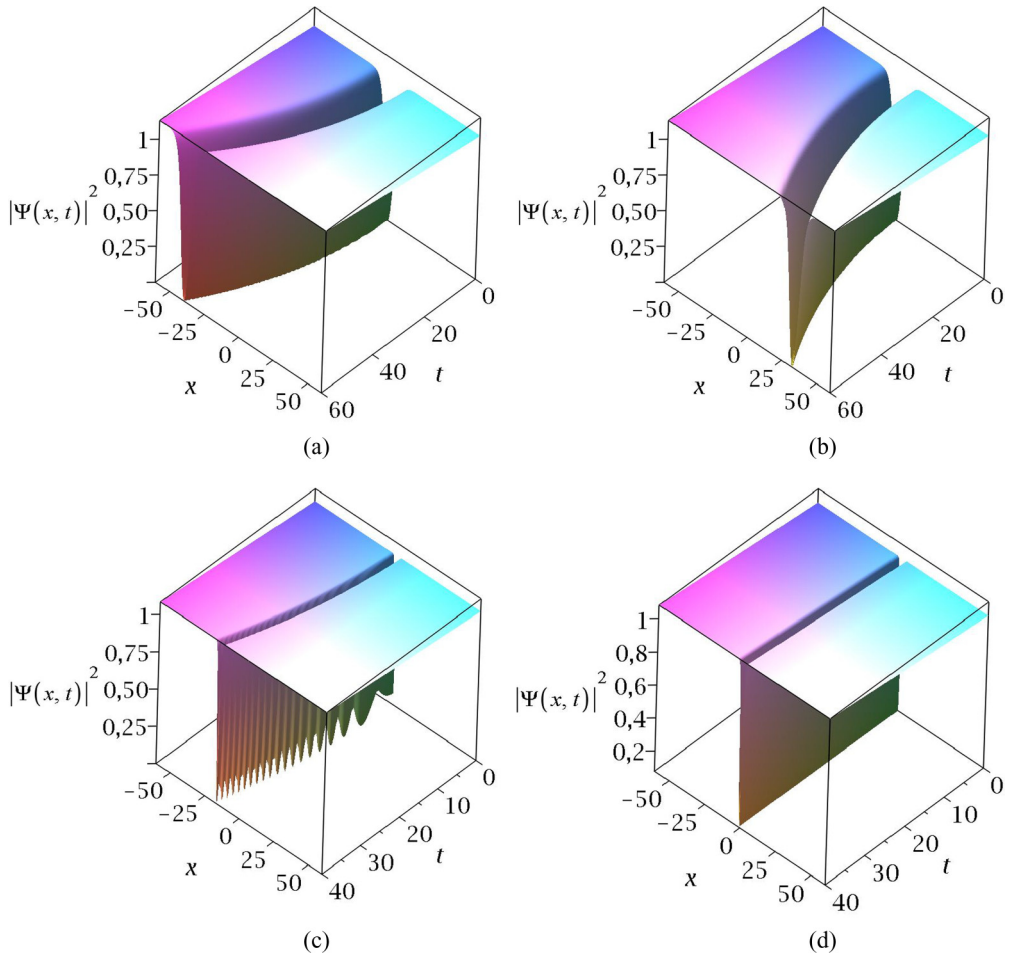

FIG. 3. (Color online) Dark profile solutions of Eq. (12), with $j = 11$, $b_0 = -4$, $b_2 = -4$, $b_4 = 4$, $b_6 = 4$, $\gamma = 0.001$, and $C_3 = 0.1$. (a) $\lambda = 0.01$; (b) $\lambda = -0.01$. The linear potential affects the direction of propagation of the soliton. (c) Small amplitudes oscillation induced by the linear potential, $W = 2$. (d) $\lambda = 0$, $W = 2$, absence of amplitude modulations when the linear potential is turned off.

B. Dark profile solutions

Equation (12) has a dark profile solution for $j = 11$, with $b_0 = -4$, $b_2 = -4$, $b_4 = 4$ (repulsive BEC), $b_6 = 4$, $\gamma = 0.001$, and $C_3 = 0.1$. We display in Fig. 3 the dynamics of dark profile patterns for two different values of the linear potential's strength λ [see panels (a) and (b)]. The BEC is drifted towards the $-x$ direction when λ is positive [see Fig. 3(a) with $\lambda = 0.01$], while the BEC evolves towards the $+x$ direction for a negative value of λ [see Fig. 3(b) with $\lambda = -0.01$], in conformity with Eq. (13). The linear potential may be used to control the direction of propagation of solitons. A similar effect has been reported in Refs. [36,50]. In addition, the dark soliton exhibits small amplitude modulations as time increases. The amplitude modulations appear earlier with smaller widths of the solitons. This feature is presented in Fig. 3(c) where $W = 2$. These amplitude modulations are completely absent when the linear potential is turned out as depicted in Fig. 3(d), where the same parameters as in Fig. 3(c) are used except $\lambda = 0$. Thus, the linear potential also induces a breathing mode behavior for which occurrence is sensitive to the width of the soliton.

The free parameters C_4 and C_2 also influence the dynamical behavior of the condensate. We turn the linear potential out in order to facilitate interpretations, and fix γ and C_3 as in Fig. 3(d). A positive value of C_4 drifts the BEC towards the $+x$ direction as confirmed by Fig. 4(a) where $C_4 = 0.035$, while a negative value of C_4 pushes the BEC towards the $-x$ direction as one can see in Fig. 4(b) where $C_4 = -0.035$. The condensate moves at a constant velocity $\dot{x} = 0.07$. One also notices in Figs. 4(a) and 4(b) that C_4 also induces small amplitude modulations. In order to check the impact of the parameter C_2, we set $C_4 = 0$. The condensate stands at position $x = \frac{-C_2}{C_3} = -2C_2$, a characteristic illustrated in Fig. 4(c) ($C_2 = 5$) and in Fig. 4(d) ($C_2 = -5$). Results presented above prove that the free parameters C_4, C_3, and C_2 can be used to manipulate the position, the velocity (C_4 only), and the width (C_3) of the BEC. Combining values of C_4, C_3, C_2, and that of λ will allow one to manipulate many features of the condensate. We plot in Fig. 4(e) the spatiotemporal evolution of the condensate's density (as an example) with $\lambda = 0.001$, $C_4 = -0.3$, $C_3 = 0.5$, and $C_2 = 0.5$. The direction, velocity, and acceleration of the condensate are tuned by an adequate selection of the parameters C_4, C_3, C_2, and λ.

C. Bright profile solutions

Bright pattern solutions are formed and displayed in Fig. 5. In Fig. 5(a) [as in Eq. (12)] we set $j = 1$ and $p = 1$, with

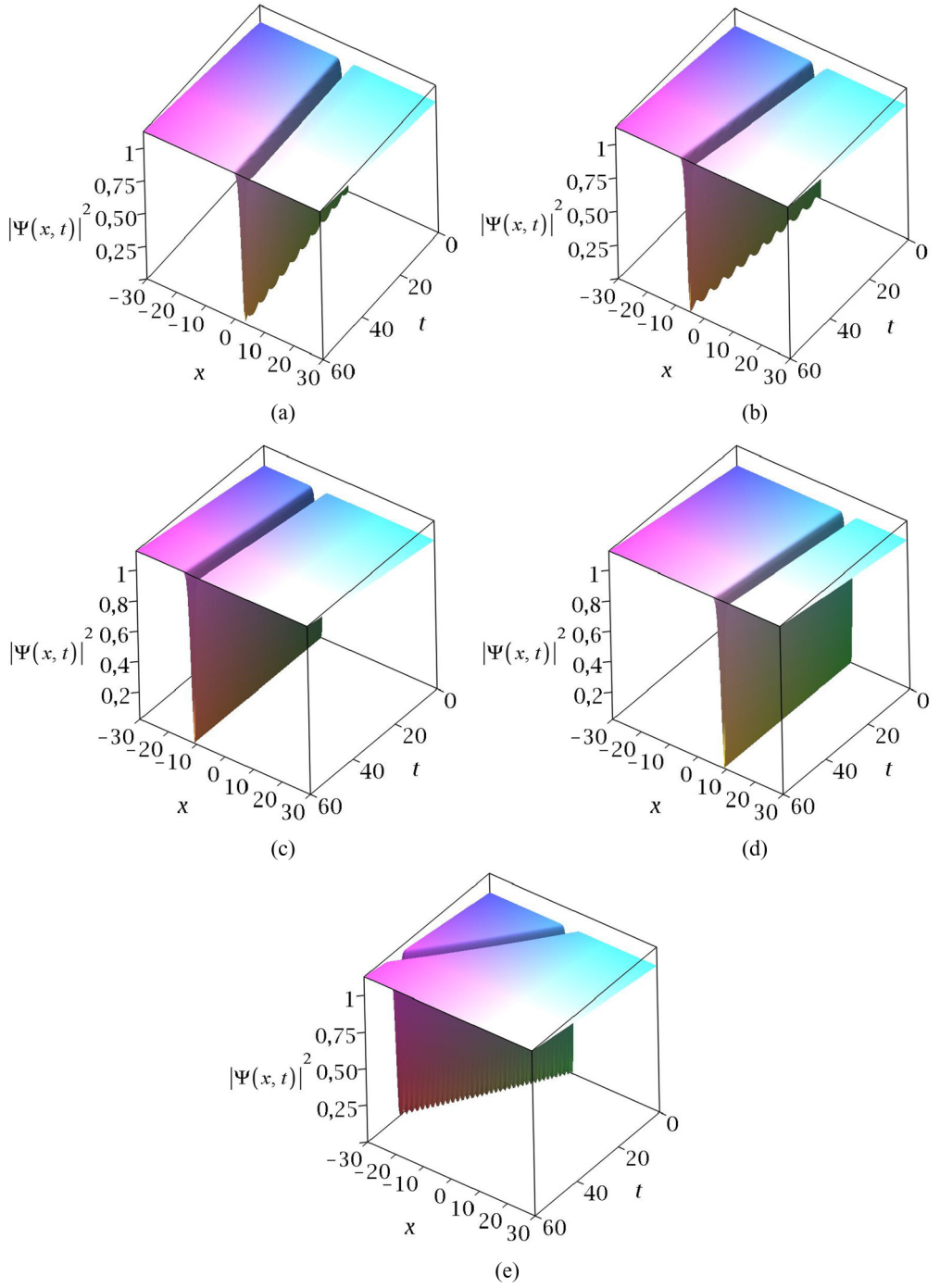

FIG. 4. (Color online) Panel (a) with $C_4 = 0.035$, and panel (b) $C_4 = -0.035$ prove that the free parameter C_4 deeply affects the direction of propagation of the wave function, and also induces a breathing mode behavior ($C_2 = 0$). Panel (c) with $C_2 = 5$, and panel (d) $C_2 = -5$ illustrate the influence that C_2 has on the direction of propagation of the wave function ($C_4 = 0$). (e) $\lambda = 0.001$, $C_4 = -0.3$, and $C_2 = C_1 = 0.5$. The other parameters are the same as in Fig. 3(d).

$b_2 = 2$, $b_4 = -3$ (attractive condensate), $b_6 = -2$, with the other parameters the same as in Fig. 1. A bright structure describing a parabola in the plane (t,x) is formed, and evolves at the constant acceleration $\ddot{x} = 0.002$. In addition, Fig. 5(b) portrays another bright matter-wave condensate obtained by setting $j = 10$, $b_2 = 2$, $b_4 = 0$ [as in Eq. (12)], with the other parameters corresponding to those in Fig. 1. The cubic nonlinearity is defocusing (repulsive), while the quintic nonlinearity is focusing (attractive).

D. Anti-kink-like and kinklike profile solutions

Another interesting solution is the anti-kink-like solution [see Fig. 6(a)] obtained for $j = 3$, $p = 1$ in Eq. (12), with $b_2 = 2$, $b_4 = -4$, $b_6 = b_4^2/4b2$, and $\gamma = 0.001$; the other

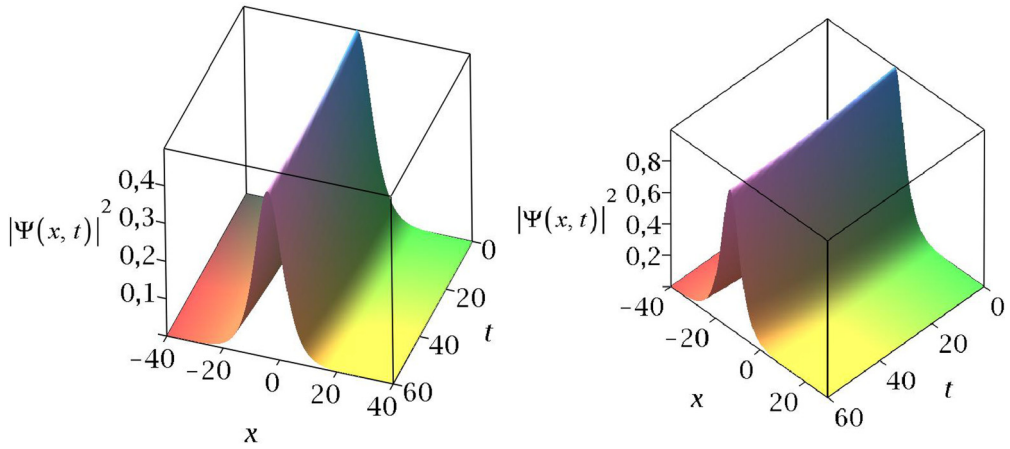

FIG. 5. (Color online) Spatiotemporal evolution of the density $|\Psi(x,t)|^2$ of bright solitons. (a) In Eq. (12), $j = p = 1$, $b_2 = 2$, $b_4 = -3$, and $b_6 = -2$. (b) In Eq. (12), $j = 10$, $b_2 = 2$, $b_4 = 0$, and the other parameters are fixed as in Fig. 1, with $\lambda = 0.001$.

parameters are as in Fig. 3(c). The argument of the tanh function is $-\sqrt{b_2}\xi$. The kinklike [see Fig. 6(b)] structure is obtained with the same parameters as in Fig. 6(a) except that the argument of the tanh function is $+\sqrt{b_2}\xi$. These solutions are displaced at the constant acceleration $\ddot{x} = 0.002$.

III. LINEAR STABILITY ANALYSIS

In the previous section, we have constructed exact solutions of Eq. (1). However, real physical systems present some perturbations. One has to analyze the stability of exact solutions found with a mathematical treatment. We analyze the stability of our solutions by linearizing the exact solution of Eq. (1) around a small perturbation. Let us consider a perturbed solution of Eq. (1) written as

$$\Psi(x,t) = [\Psi_1(x,t) + \Psi_2(x,t)] \exp[\imath\theta(x,t)], \qquad (15)$$

where $\Psi_1(x,t)\exp[\imath\theta(x,t)]$ is the exact solution of Eq. (1), and $\Psi_2(x,t) = R(x,t) + \imath I(x,t)$ represents a small perturbation, i.e., $|\Psi_2(x,t)|^2 \ll |\Psi_1(x,t)|^2$. Inserting Eq. (15) into Eq. (1) and linearizing around the perturbation, we derive the following system of equations:

$$\begin{aligned} R_t &= -I_{xx} + \big[\theta_t + \theta_x^2 + g(t)\Psi_1(x,t)^2 \\ &\quad + \chi(t)\Psi_1(x,t)^4 + \lambda x\big] I + (\theta_{xx} + \gamma)R - 2\theta_{xx} I_x, \\ I_t &= R_{xx} - \big[\theta_t + \theta_x^2 + 3g(t)\Psi_1(x,t)^2 + 5\chi(t)\Psi_1(x,t)^4 + \lambda x\big] \\ &\quad \times R - (\theta_{xx} - \gamma)I - 2\theta_{xx} I_x. \end{aligned} \qquad (16)$$

The analysis of the linear problem (16) is a nontrivial task, so we only focus on solutions with zero spatial frequency shift, i.e., $\Gamma(t) = 0$. This implies that $\lambda = 0$, $C_4 = 0$, $\ddot{x} = \dot{x} = 0$, $\eta = C_2$, $\xi(x,t) \equiv \xi(x) = C_3 x + C_2$, $\theta_t = 2b_2 C_3^2$, and $\theta_x = \theta_{xx} = 0$. As in all solutions plotted above, we set $C_1 = 0$; the homogenous phase becomes $\Omega(t) = 2b_2 C_3^2 t$. Following the work in Ref. [51], we rewrite the system (16) in this form:

$$\begin{pmatrix} R_t \\ I_t \end{pmatrix} = J \begin{pmatrix} L_+ & -S \\ S & L_- \end{pmatrix} \begin{pmatrix} R \\ I \end{pmatrix}. \qquad (17)$$

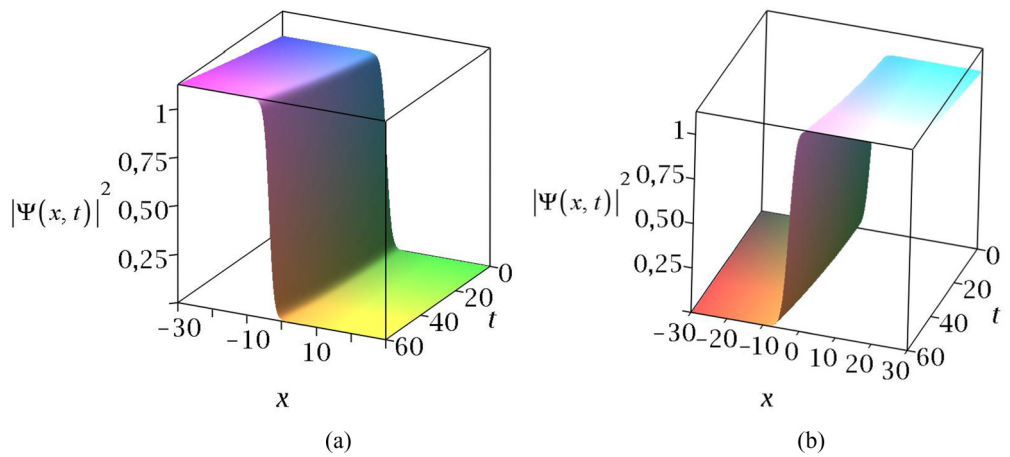

FIG. 6. (Color online) Spatiotemporal evolution of the density $|\Psi(x,t)|^2$ of anti-kink-like and kinklike pattern solutions of Eq. (12). (a) Anti-kink-like solution. (b) Kinklike solution. The parameters are $j = 3$, $p = 1$, $b_2 = 2$, $b_4 = -4$, $b_6 = b_4^2/4b_2$, $\gamma = 0.001$, $\lambda = 0.001$, and the other parameters taken as in Fig. 3(c).

In Eq. (17) $J = \left(\begin{smallmatrix} 0 & 1 \\ -1 & 0 \end{smallmatrix}\right)$ and

$$L- = -\frac{\partial^2}{\partial x^2} + 2b_2C_3^2 + g(t)\Psi_1(x,t)^2 + \chi(t)\Psi_1(x,t)^4 + \lambda x,$$

$$L_+ = -\frac{\partial^2}{\partial x^2} + 2b_2C_3^2 + 3g(t)\Psi_1(x,t)^2 + 5\chi(t)\Psi_1(x,t)^4 + \lambda x,$$

$$S = \gamma. \tag{18}$$

We assume that the perturbation takes the form

$$R(x,t) = r_1(x)\exp(\beta t),$$
$$I(x,t) = r_2(x)\exp(\beta t). \tag{19}$$

Substituting Eq. (19) into Eq. (17) yields an eigenvalue problem given by

$$J\begin{pmatrix} L_+ & -\gamma \\ \gamma & L_- \end{pmatrix}\begin{pmatrix} r_1 \\ r_2 \end{pmatrix} = \beta\begin{pmatrix} r_1 \\ r_2 \end{pmatrix}. \tag{20}$$

This linear stability procedure can be applied to all solutions of Eq. (1) given by Eq. (12). However, one has to check the stability of each solution step by step since the functions $\phi(\xi)$ are different. We consider as examples, the cases of the periodic, antikink, kink, and dark solitons presented above. Exploiting theorems presented in [51] and applied in [10,51–54], we arrive at the following conclusions:

(i) Since in Eq. (12), for $j = 2$, $p = 1$ the function $h(t)\phi(\xi) > 0$, the homogeneous phase periodic solution is linearly stable in a repulsive BEC.

(ii) The homogeneous anti-kink-like and kinklike solitons are linearly stable in a repulsive BEC.

(iii) The homogeneous dark soliton is linearly unstable in the attractive BEC.

IV. NUMERICAL SIMULATIONS

The main subject of this part is to test the validity of the exact solutions found above. For solutions derived with approximate methods such as the one adopted here, comparisons with direct numerical integrations of the original equation are usually necessary. The reason is that an exact analytical solution may lead to wrong results if the initial condition is not close to the exact numerical solution. For instance, exact analytical solutions obtained via the standard variational approximation widely used to study properties of solitons in BECs are always compared with their numerical counterparts [55]. In this part of the work, we emphasize that our exact analytical solutions do not deviate from the numerical ones by showing at particular times the agreement between both solutions. Due to the presence of the complex potential, Eq. (1) is a dissipative GPE. Hence, the localized matter-wave structures found above are the well-known dissipative solitons, where gain, loss, dispersion, and nonlinearities are balanced during numerical simulations. The extended period of time numerical behavior of our dissipative soliton solutions definitely implies that they may be used for convenient comparison with current or future experiments. Starting from

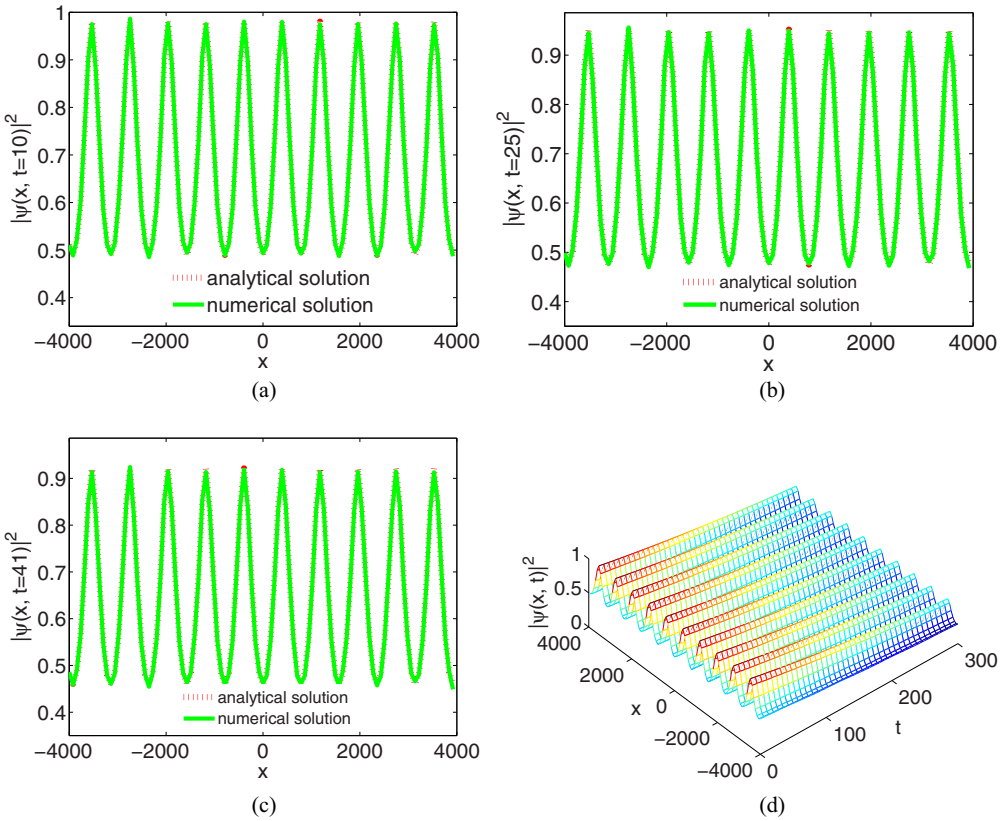

FIG. 7. (Color online) (a)–(c) Spatial comparison between the numerical (solid line) and the analytical (dotted line) periodical solutions of (12) for $j = 2$, $p = 1$. (d) Stable density profile of the periodic solution. In all panels, parameters are the same as in Fig. 2(a), except $W = 400$. Both numerical and analytical solutions agree with a very high accuracy.

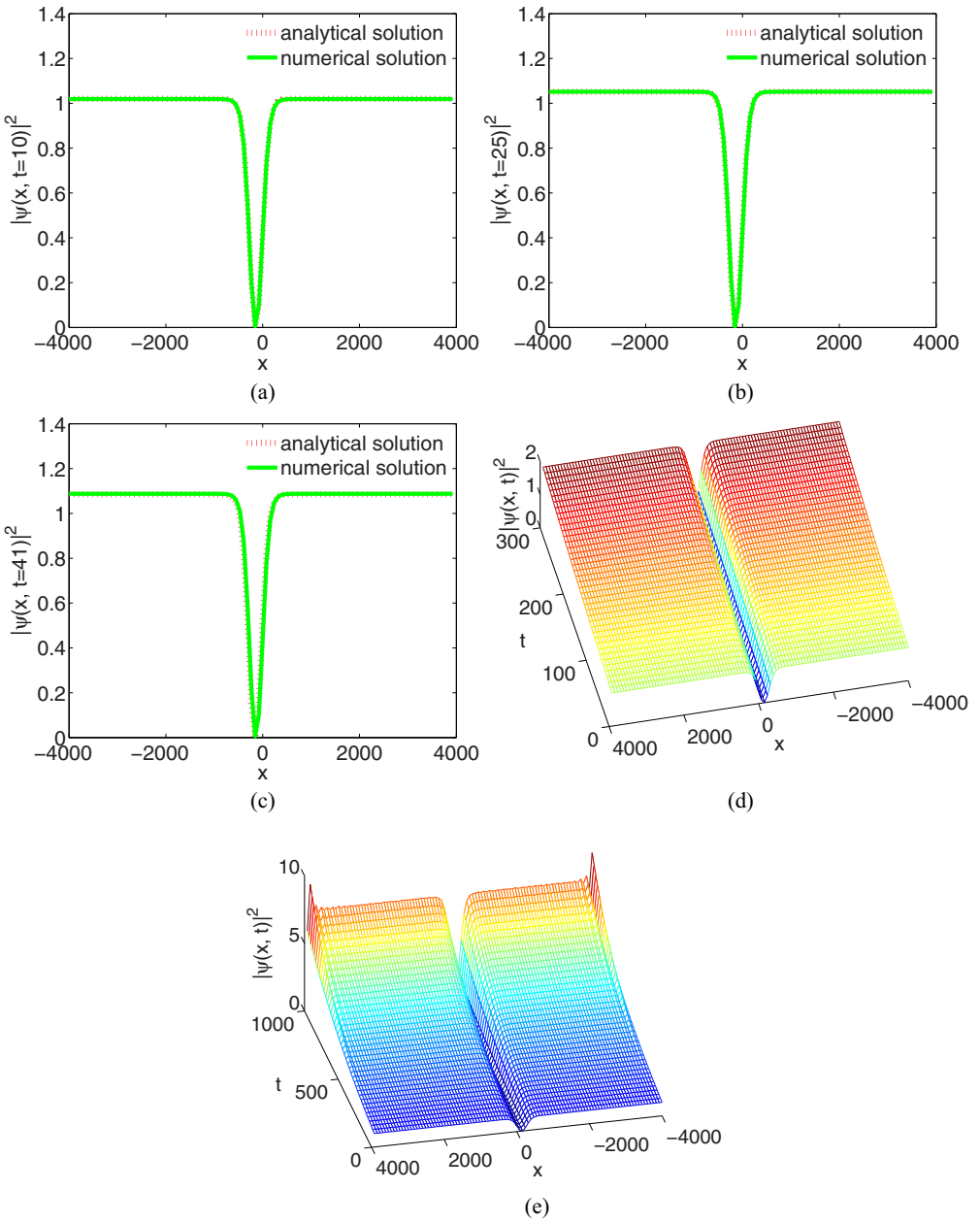

FIG. 8. (Color online) (a)–(c) Spatial comparison between the numerical (solid line) and the analytical (dotted line) dark solutions of (12) for $j = 11$. (d) Stable propagation of the dark soliton. In all panels, parameters are the same as in Fig. 3(a), except $W = 400$. (e) Spatiotemporal evolution of the trivial phase dark profile solution with only very small amplitude oscillations at the top.

the same initial conditions, we show that the analytic and numerical solutions agree well. The numerical procedure used is the fourth-order Runge-Kutta in the interaction picture method [56,57]. The spatial grid is sufficiently large in order to prevent problems with the boundaries [56,57]. Solutions are initially perturbed with a small amount of random white noise.

We insert the exact nontrivial phase (or zero spatial frequency shift) solution of Fig. 2(a) through Eq. (1), at time $t = 0$. The width of the solution is set to $W = 400$, for clarity. Figures 7(a)–7(c) depict the spatial variation of the density at different times. One observes that the exact numerical solution also leads to a periodic solution with the same width and the same spatial period. The agreement between the numerical result and the analytical one, as presented in Figs. 7(a)–7(d), is very good, though with the addition of a small initial random white noise. The periodic nontrivial phase solution, as one can realize in Fig. 7(d), is not only linearly stable but also dynamically stable. In Figs. 8(a)–8(c), we display the comparison between the analytical nontrivial phase solution of Fig. 3(a), and the exact numerical solution at different times. For the sake of clarity, we have changed the value of the width which is now $W = 400$. As time increases, the agreement between the analytical and the numerical exact solutions is quite good. The nontrivial phase dark profile solution is also

linearly and dynamically stable. We also investigate the linear and dynamical stability of the dark trivial phase solution. Following the analytical study carried out above, we find the linear potential, i.e., $\lambda = 0$, and set the free parameters as in Fig. 8(a). Then, the dark profile trivial phase solution is injected through the system. We display in Fig. 8(e) the spatiotemporal evolution of the density of the wave function. One realizes that the dark trivial phase solution preserves its shape as time increases. However, at the top of the dark trivial phase solution, we observe benign random oscillations. This is a signature of the presence of small instabilities which are consistent with the linear stability analysis carried out above. However, these instabilities do not drastically develop such that the dark trivial phase solution is numerically robust. Moreover, the bright nontrivial phase profile solution of Fig. 5(a) with $W = 400$ is also numerically stable. We exhibit in Figs. 9(a)– 9(c) a parallel between the analytical prediction and the numerical exact solutions [of solution of Fig. 5(a)], which correctly match each other. In addition, we also perform full numerical simulations of the bright profile solution displayed in Fig. 5(b) with $W = 400$, then compare the results with their analytical counterparts in Figs. 9(e)–9(h), and observe very good agreements. As in the case of the periodic solution, the small perturbation introduced at the initial time does not alter the integrity of the nontrivial phase bright soliton solutions. Considering the nontrivial phase anti-kink-like and the kinklike solutions presented in Fig. 6, except for the width fixed as $W = 400$, panels (a)–(d) for the anti-kink solution and panels (e)–(h) for the kink solution show good agreement between the numerical and the analytical predictions (see Fig. 10). There are very small amplitude instabilities that set in the system. However, the impact of these instabilities is not drastic since the shapes of the anti-kink-like and the kinklike solutions persist at longer times. Thus, both the anti-kink-like and the kinklike solutions are dynamically stable. In the cases of the trivial phase dark solution as well as the nontrivial phase anti-kink-like and kinklike solutions, we recall the existence of very small instabilities, such that in the point of view of mathematics, the latter solutions are unstable. Since the instabilities develop very slowly over time, one can say that these solutions can be physically stable.

V. CONCLUSION

In this work, we have studied the cubic-quintic GPE with time-dependent two- and three-body nonlinearities, trapped in a linear potential and exchanging atoms with the thermal cloud. Using the Lenard equation [Eq. (3)] with the extended tanh-function method, we have derived 22 exact solutions of Eq. (1), which include periodic solutions, dark profile solutions, bright profile solutions, anti-kink-like and kinklike profile solutions, and many others. Solutions presented in the present work apply only for special time-dependent behaviors of the two- and three-body nonlinearities provided by Eqs. (5), (8), and (9). These solutions have many free parameters which can be used to manage many features of matter-wave condensates such as the position, width, velocity, acceleration, and density. Furthermore, adjusting the strength of the linear potential is useful to control the position, the acceleration of the wave, and in certain cases induces small amplitude modulations of the localized solutions. In addition, the parameter related to the feeding (or loss) of atoms affects the height of the condensate's density by modulating the two- and the three-body interatomic interactions. Exact numerical integrations of Eq. (1) confirm the analytical predictions with a good accuracy. Furthermore, all solutions presented in this work appear to be dynamically stable. These solutions provide a way to create, manipulate, and have a better understanding of many dynamical properties of matter-wave condensates with time varying cubic-quintic nonlinearities.

Since the pioneer work on nonautonomous solitons in nonlinear Schrödinger equation types [58], many works have been devoted to the construction of new soliton solutions of nonlinear Schrödinger equation types with versatile time, space, or space-time nonlinearities [59]. In the context of BECs, a similarity transformation method has been used to construct exact soliton solutions of condensates with space-time cubic-quintic nonlinearities [59]. Additionally, in Ref. [59], the external potential that characterizes the geometry of the medium in which the condensate is trapped is a real space-time potential, which is quadratic and linear in space. This kind of potential implies a conservation of the number of atoms in the BEC. Additionally, in the work [59], soliton solutions and the shape of the trapping potential are derived for an assumed form of the cubic-quintic nonlinearities. On the contrary, in the method presented in this work, the cubic and the quintic nonlinearities are constructed meanwhile with the exact soliton solutions. Furthermore, the external potential only consists of a linear potential, with a gain or loss. Hence, the interaction between the condensed fraction of atoms and the uncondensed thermal background is taken into account in the present work. The latter interaction between the BEC and the substrate can be controlled by selecting the rate of exchange of atoms γ. Exact soliton solutions presented here are constructed with a relatively simpler method, in comparison to the similarity transformation method in [59]. The experimental realization of results obtained in this work can be easily implemented since the key parameters needed are only γ and λ. Condensates with a linear potential and with atom loss or gain have already been realized. The management of the nonlinearities may be realized in optical lattices [59], or in magnetic fields as previously mentioned.

ACKNOWLEDGMENTS

D.B.B. and T.C.K. are grateful for the hospitality of the Abdus Salam International Center for Theoretical Physics (Trieste, Italy) where a part of this work was done. D.B.B. acknowledges useful conversations with Dr. M. B. Obounou Akong and Dr. G. R. Kol. The authors thank anonymous referees for their useful suggestions.

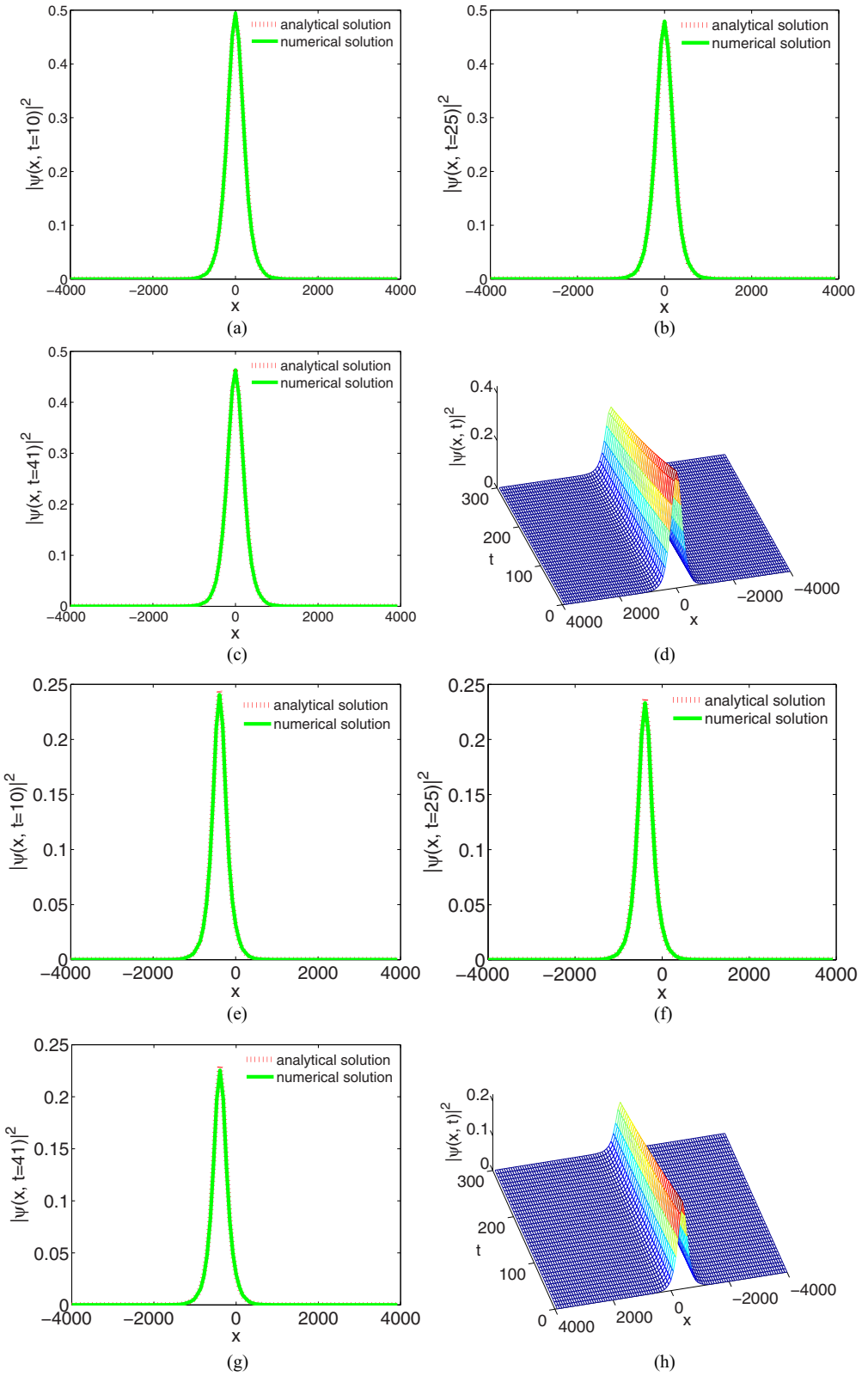

FIG. 9. (Color online) (a)–(c) and (e)–(g) Spatial comparison between the numerical (solid line) and the analytical (dotted line) bright solutions of (12). (d) and (h) Stable propagation of bright solitons. Parameters in panels (a)–(d) correspond to those in Fig. 5(a), while parameters in panels (e)–(h) correspond to Fig. 5(b), except $W = 400$. These nontrivial phase bright profile solutions remain stable during propagation.

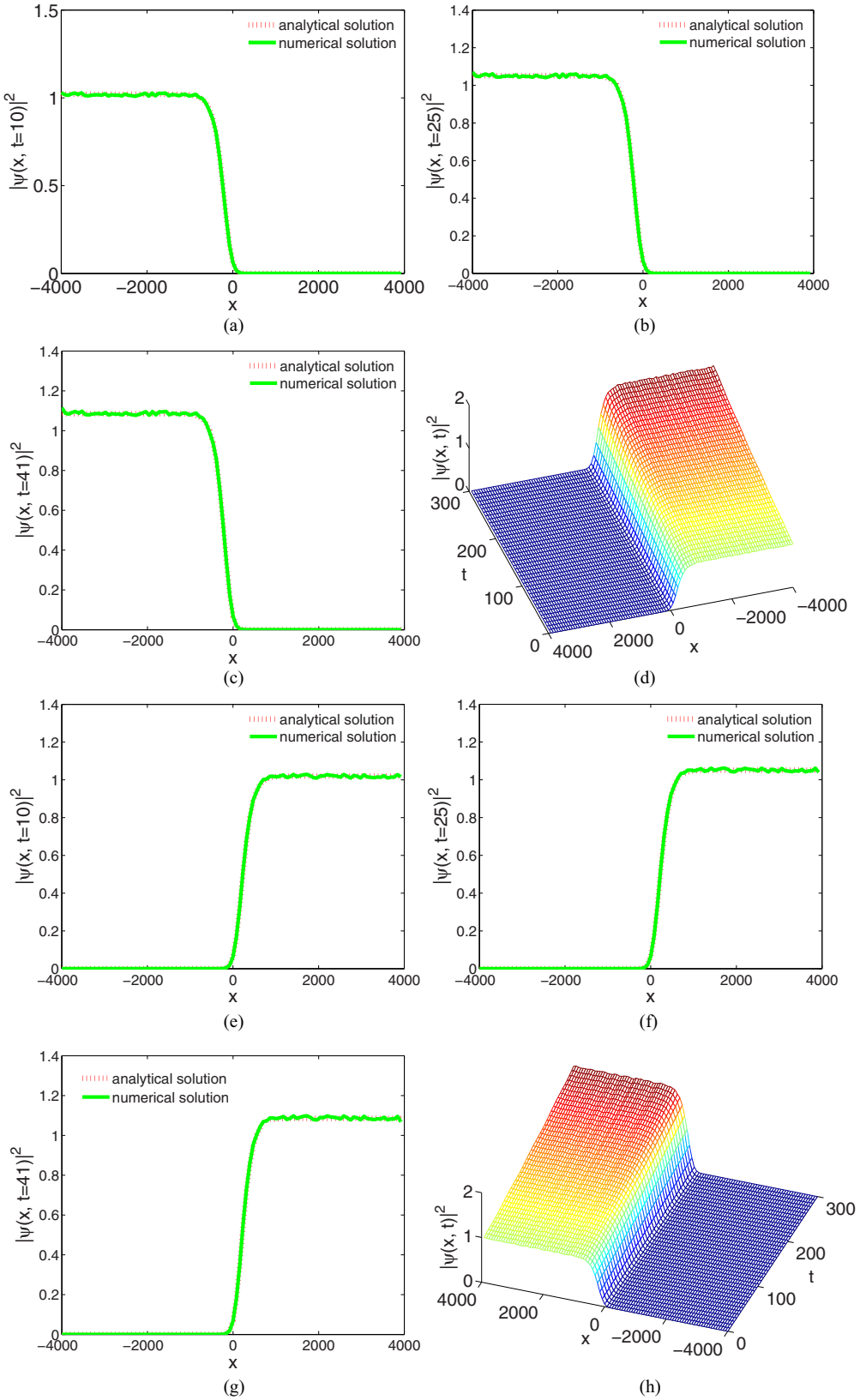

FIG. 10. (Color online) (a)–(c) and (e)–(g) Spatial comparison between the numerical (solid line) and the analytical (dotted line) anti-kink-like and kinklike solutions of Fig. 6. (d) and (h) Stable propagation of anti-kink-like and kinklike solitons, respectively. The parameters in (a)–(d) correspond to those in Fig. 6(a), while the parameters in panels (e)–(h) correspond to Fig. 6(b), except $W = 400$. Although some very small instabilities exist that appear at the top of the density profiles, both the anti-kink-like and kinklike solutions are robust and can be observed in real physical experiments.

APPENDIX: SOLUTIONS OF THE LENARD EQUATION

Given below are some solutions of the Lenard equation [Eq. (3)].

(1) $b_0 = 0, b_2 > 0, b_4 < 0, b_6 < 0, \delta = b_4^2 - 4b_2b_6 > 0$: $\phi_{11} = \sqrt{\frac{2b_2\mathrm{sech}^2(\sqrt{b_2}\xi)}{2\sqrt{\delta}-(\sqrt{\delta}+b_4)\mathrm{sech}^2(\sqrt{b_2}\xi)}}$, $\phi_{12} = \sqrt{\frac{2b_2\mathrm{csch}^2(\pm\sqrt{b_2}\xi)}{2\sqrt{\delta}+(\sqrt{\delta}-b_4)\mathrm{csch}^2(\pm\sqrt{b_2}\xi)}}$;

(2) $b_0 = 0, b_2 < 0, b_4 \geqslant 0, b_6 < 0, \delta > 0$: $\phi_{21} = \sqrt{\frac{-2b_2\sec^2(\sqrt{-b_2}\xi)}{2\sqrt{\delta}-(\sqrt{\delta}-b_4)\sec^2(\sqrt{-b_2}\xi)}}$, $\phi_{22} = \sqrt{\frac{2b_2\csc^2(\pm\sqrt{-b_2}\xi)}{2\sqrt{\delta}+(\sqrt{\delta}+b_4)\csc^2(\pm\sqrt{-b_2}\xi)}}$;

(3) $b_0 = 0, b_6 = \frac{b_4^2}{4b_2}, b_2 > 0, b_4 < 0$: $\phi_{31} = \sqrt{\frac{-b_2}{b_4}[1+\tanh(\pm\sqrt{b_2}\xi)]}$, $\phi_{32} = \sqrt{\frac{-b_2}{b_4}[1+\coth(\sqrt{b_2}\xi)]}$;

(4) $b_0 = 0, b_2 > 0$: $\phi_{41} = \sqrt{\frac{-b_2b_4\mathrm{sech}^2(\sqrt{b_2}\xi)}{b_4^2-b_2b_6[1+\tanh^2(\sqrt{b_2}\xi)]}}$, $\phi_{42} = \sqrt{\frac{b_2b_4\mathrm{csch}^2(\sqrt{b_2}\xi)}{b_4^2-b_2b_6[1+\coth^2(\sqrt{b_2}\xi)]}}$, $\phi_{43} = 4\sqrt{\frac{b_2\exp(2\sqrt{b_2}\xi)}{\exp(4\sqrt{b_2}\xi-4C_4)-64b_2b_6}}$;

(5) $b_0 = 0, b_2 > 0, \delta > 0$: $\phi_5 = \sqrt{\frac{2b_2}{\sqrt{\delta}\cosh(2\sqrt{b_2}\xi)-b_4}}$;

(6) $b_0 = 0, b_2 > 0, \delta < 0$: $\phi_6 = \sqrt{\frac{2b_2}{\sqrt{-\delta}\sinh(2\sqrt{b_2}\xi)-b_4}}$;

(7) $b_0 = 0, b_2 < 0, \delta > 0$: $\phi_7 = \sqrt{\frac{2b_2}{\sqrt{\delta}\sin(2\sqrt{-b_2}\xi)-b_4}}$;

(8) $b_0 = 0, b_2 > 0, b_6 > 0$: $\phi_{81} = \sqrt{\frac{-b_2\mathrm{sech}^2(\sqrt{b_2}\xi)}{b_4+2\sqrt{b_2b_6}\tanh(\sqrt{b_2}\xi)}}$, $\phi_{82} = \sqrt{\frac{b_2\mathrm{csch}^2(\sqrt{b_2}\xi)}{b_4+2\sqrt{b_2b_6}\coth(\sqrt{b_2}\xi)}}$;

(9) $b_0 = 0, b_2 < 0, b_6 > 0$: $\phi_{91} = \sqrt{\frac{-b_2\sec^2(\sqrt{-b_2}\xi)}{b_4+2\sqrt{-b_2b_6}\tan(\sqrt{-b_2}\xi)}}$, $\phi_{92} = \sqrt{\frac{-b_2\csc^2(\sqrt{-b_2}\xi)}{b_4+2\sqrt{-b_2b_6}\cot(\sqrt{-b_2}\xi)}}$;

(10) $b_0 = 0, b_2 > 0, b_4 = 0$: $\phi_{10} = 4\sqrt{\frac{\pm b_2\exp(2\sqrt{b_2}\xi)}{1-64b_2b_6\exp(4\sqrt{b_2}\xi)}}$;

(11) $b_0 = -4, b_4 = -4, b_6 = 4$: $\phi_{11} = \pm\imath\frac{\tanh(2\sqrt{2}\xi+1)}{\sqrt{2-\tanh^2(2\sqrt{2}\xi)+1}}$

[1] M. H. Anderson, J. R. Ensher, M. R. Mathews, C. E. Wieman, and E. A. Cornell, Science **269**, 198 (1995).
[2] C. C. Bradley, C. A. Sackett, J. J. Tollett, and R. G. Hulet, Phys. Rev. Lett. **75**, 1687 (1995).
[3] K. B. Davis, M.-O. Mewes, M. R. Andrews, N. J. van Druten, D. S. Durfee, D. M. Kurn, and W. Ketterle, Phys. Rev. Lett. **75**, 3969 (1995).
[4] I. Bloch, J. Dalibard, and W. Zwerger, Rev. Mod. Phys. **80**, 885 (2008).
[5] F. K. Abdullaev, P. G. Kevrekidis, and M. Salerno, Phys. Rev. Lett. **105**, 113901 (2010).
[6] V. N. Serkin, A. Hasegawa, and T. L. Belyaeva, Phys. Rev. Lett. **98**, 074102 (2007).
[7] H. M. Li and F. Q. Song, Opt. Commun. **277**, 174 (2007).
[8] E. Fan, Phys. Lett. A **277**, 212 (2000).
[9] E. Yomba, Phys. Lett. A **336**, 463 (2005).
[10] A. Mohamadou, E. Wamba, D. Lissouck, and T. C. Kofane, Phys. Rev. E **85**, 046605 (2012).
[11] J. L. Roberts, N. R. Claussen, J. P. Burke, C. H. Greene, E. A. Cornell, and C. E. Wieman, Phys. Rev. Lett. **81**, 5109 (1998).
[12] J. Stenger, S. Inouye, M. R. Andrews, H.-J. Miesner, D. M. Stamper-Kurn, and W. Ketterle, Phys. Rev. Lett. **82**, 2422 (1999).
[13] D. E. Pelinovsky, P. G. Kevrekidis, and D. J. Frantzeskakis, Phys. Rev. Lett. **91**, 240201 (2003).
[14] S. Inouye, M. R. Andrews, J. Stenger, H. J. Miesner, D. M. Stamper-Kurn, and W. Ketterle, Nature (London) **392**, 151 (1998).
[15] E. B. Kolomeisky, T. J. Newman, J. P. Straley, and X. Qi, Phys. Rev. Lett. **85**, 1146 (2000).
[16] F. K. Abdullaev and J. Garnier, Phys. Rev. A **70**, 053604 (2004).
[17] H. P. Büchler, A. Micheli, and P. Zoller, Nat. Phys. **3**, 726 (2007).
[18] B. Paredes, T. Keilmann, and J. I. Cirac, Phys. Rev. A **75**, 053611 (2007).
[19] F. Kh. Abdullaev, A. A. Abdumalikov, and R. M. Galimzyanov, Phys. Lett. A **367**, 149 (2007).
[20] U. Al. Khawaja, J. Phys. A: Math. Theor. **39**, 9679 (2006).
[21] K. D. Moll, A. L. Gaeta, and G. Fibich, Phys. Rev. Lett. **90**, 203902 (2003).
[22] P. K. Kevrekidis and D. J. Frantzeskakis, Mod. Phys. Lett. B **18**, 173 (2004).
[23] V. M. Perez-García, V. V. Konotop, and V. A. Brazhnyi, Phys. Rev. Lett. **92**, 220403 (2004).
[24] A. E. Leanhardt, A. P. Chikkatur, D. Kielpinski, Y. Shin, T. L. Gustavson, W. Ketterle, and D. E. Pritchard, Phys. Rev. Lett. **89**, 040401 (2002).
[25] T. Köhler, Phys. Rev. Lett. **89**, 210404 (2002).
[26] P. Pieri and G. C. Strinati, Phys. Rev. Lett. **91**, 030401 (2003).
[27] B. Laburthe Tolra, K. M. O'Hara, J. H. Huckans, W. D. Phillips, S. L. Rolston, and J. V. Porto, Phys. Rev. Lett. **92**, 190401 (2004).
[28] J. Söding, D. Guéry-Odelin, P. Desbiolles, F. Chevy, H. Inamori, and J. Dalibard, Appl. Phys. B: Lasers Opt. **69**, 257 (1999).
[29] U. Roy, R. Atre, C. Sudheesh, C. N. Kumar, and P. K. Panigrahi, J. Phys. B: At. Mol. Opt. Phys. **43**, 025003 (2010).
[30] A.-X. Zhang and J.-K. Xue, Phys. Rev. A **75**, 013624 (2007).
[31] Yu. Kagan, A. E. Muryshev, and G. V. Shlyapnikov, Phys. Rev. Lett. **81**, 933 (1998).
[32] V. S. Filho, S. M. Holz, and L. Tomio, Phys. Lett. A **372**, 6778 (2008).
[33] B. Kneer, T. Wong, K. Vogel, W. P. Schleich, and D. F. Walls, Phys. Rev. A **58**, 4841 (1998), and references therein.
[34] V. A. Brazhnyi, V. V. Konotop, V. M. Pérez-García, and H. Ott, Phys. Rev. Lett. **102**, 144101 (2009).
[35] N. P. Proukakis and B. Jackson, J. Phys. B: At. Mol. Opt. Phys. **41**, 203002 (2008).
[36] E. Wamba, T. C. Kofané, and A. Mohamadou, Chin. Phys. B **21**, 070504 (2012).
[37] E. Kengne and P. K. Talla, J. Phys. B: At. Mol. Opt. Phys. **39**, 3679 (2006).
[38] C. C. Bradley, C. A. Sackett, J. H. Tollett, and R. G. Hulet, Phys. Rev. Lett. **79**, 1170(E) (1997).

[39] L. Khaykovich, F. Schreck, G. Ferrari, T. Bourdel, J. Cubizolles, L. D. Carr, Y. Casting, and C. Salomon, Science **296**, 1290 (2002).
[40] K. E. Strecker, G. B. Partridge, A. G. Truscott, and R. G. Hulet, Nature (London) **417**, 150 (2002).
[41] Q. Y. Li, Z. D. Li, Lu Li, and G. S. Fu, Opt. Commun. **283**, 3361 (2010).
[42] S. Sabari, R. V. J. Raja, K. Porsezian, and P. Murugunandam, J. Phys. B: At. Mol. Opt. Phys. **43**, 125302 (2010).
[43] J. Zeng and B. A. Malomed, Phys. Rev. A **85**, 023824 (2012).
[44] V. S. Filho, T. Frederico, A. Gammal, and L. Tomio, Phys. Rev. E **66**, 036225 (2002).
[45] L. Tomio, V. S. Filho, A. Gammal, and T. Frederico, Nucl. Phys. A **684**, 681 (2001).
[46] K. W. Chow, C. K. Lam, K. Nakkeeran, and B. A. Malomed, J. Phys. Soc. Jpn. **77**, 054001 (2008).
[47] D. Belobo Belobo, G. H. Ben-Bolie, T. B. Ekogo, C. G. Latchio Tiofack, and T. C. Kofane, Int. J. Mod. Phys. B **26**, 1250164 (2012).
[48] O. Morsch and M. Oberthaler, Rev. Mod. Phys. **78**, 179 (2006).
[49] G. K. Campbell, Ph.D. thesis, MIT, 2006.
[50] D. Belobo Belobo, G. H. Ben-Bolie, and T. C. Kofane, Phys. Rev. E (to be published).
[51] J. C. Bronski, L. D. Carr, B. Deconinck, and J. N. Kutz, Phys. Rev. Lett. **86**, 1402 (2001).
[52] J. C. Bronski, L. D. Carr, B. Deconinck, J. N. Kutz, and K. Promislow, Phys. Rev. E **63**, 036612 (2001).
[53] B. Deconinck, B. A. Frigyik, and J. N. Kutz, Phys. Lett. A **283**, 177 (2001).
[54] E. Kengne, X. X. Liu, B. A. Malomed, S. T. Chui, and W. M. Liu, J. Math. Phys. **49**, 023503 (2008).
[55] D. Belobo Belobo, T. B. Ekogo, G. H. Ben-Bolie, and T. C. Kofané, Far East J. Dynam. Syst. **16**, 107 (2011), and references therein.
[56] B. M. Caradoc-Davies, R. J. Ballagh, and K. Burnett, Phys. Rev. Lett. **83**, 895 (1999).
[57] B. M. Caradoc-Davies, R. J. Ballagh, and P. B. Blakie, Phys. Rev. A **62**, 011602(R) (2000).
[58] V. N. Serkin and A. Hasegawa, Phys. Rev. Lett. **85**, 4502 (2000), and references therein.
[59] A. T. Avelar, D. Bazeia, and W. B. Cardoso, Phys. Rev. E **79**, 025602(R) (2009), and references therein.